Laser driven x-ray imaging of human trabecular bone

Contact *j.cole11@imperial.ac.uk*

J. M. Cole, J. Wood, K. Poder, J. Bryant, S. Alatabi, K. Mecseki, S. Kneip, S. P. D. Mangles, Z. Najmudin
The John Adams Institute for Accelerator Science Imperial College London, SW7 2AZ, UK

N. Lopes

The John Adams Institute for Accelerator Science Imperial College London, SW7 2AZ, UK

GoLP, Instituto Superior Tecnico, Lison, Portugal

R. Abel, A. Jin

MSK Laboratory, Charing Cross Hospital, Imperial College London, W6 8RF, UK

D. R. Symes

Central Laser Facility, STFC Rutherford Appleton Laboratory, Chilton, Didcot, OX11 0QX, UK

Introduction

There is a pressing need in both histological and diagnostic medical imaging to be able to examine the structure of human bone on the micron level[1–3]. Trabecular bone is the spongy and porous bone layer responsible for most internal metabolic activity and red blood cell production. Due to the high rate of bone calcium turnover there, trabecular bone is affected severely by osteodegenerative diseases such as osteoporosis[4], leading to the appearance of microcracks[5] and thinning or broken trabeculae. Detecting these characteristic early signs of osteoporosis in the bone would help in diagnosis and state of the art clinical drug trials[6]. The complex, small scale structure and high atomic density of trabecular bone places stringent demands on any proposed x-ray source – it should be high energy, have a small source size and produce a relatively high flux of photons.

Microfocus x-ray sources are commonly used in clinical settings[7], producing Kα and bremsstrahlung x-rays by focussing an electron beam onto a high-Z metal anode. Unfortunately the achievable x-ray flux is limited by the melting point of the anode – focussing the electron beam to reduce the source size heats the anode. If the anode is to stay solid the electron flux, and hence x-ray flux, must be reduced[8].

The laser-wakefield acceleration (LWFA) technique[9–11] relies instead on a plasma to accelerate electrons longitudinally and transversely, acting as both the accelerating and radiating[12] medium. As a consequence it is possible to generate tightly focussed and high current electron beams without damaging any 'target' material, and the dependence of x-ray flux on source size is lifted. Here we demonstrate the use of a laser-wakefield driven x-ray source to take high-resolution absorption contrast radiographs of a human femoral trabecular bone sample in single shots.

Experimental Setup

The experiment described here took place at the Astra-Gemini laser facility[13], which delivered pulse energies of 11.4 ± 0.4 J in 45 fs at 800 nm. The 150 mm diameter linearly-polarised Gemini beam was focussed with a 3 m focal length (*f*/20) parabolic mirror into a slightly elliptical focal spot of 25×32 μm FWHM. The peak laser intensity at vacuum focus was then $(1.80 \pm 0.6) \times 10^{19}$ Wcm^{-2}, corresponding to a normalised vector potential of $a_0 = 3.0 \pm 0.1$. This and the remainder of the electron and x-ray beamlines were installed under vacuum and are illustrated in Figure 1.

The laser was focussed onto the front of a variable-length gas cell containing pure helium gas, delivered through precisely-timed valves. By varying the relative delay between the valve opening time and the arrival time of the laser pulse it was possible to precisely control the gas pressure, and therefore plasma density. Throughout the experiment the cell length and plasma density were adjusted for best electron and x-ray beam properties.
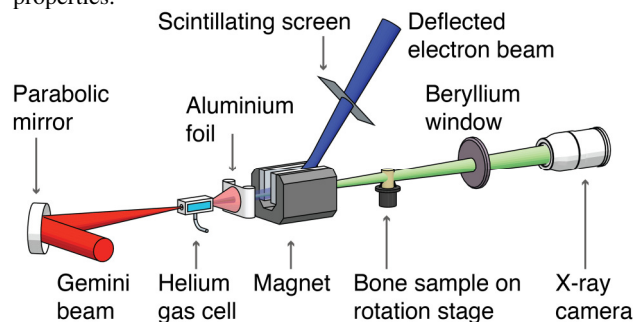
Figure 1: Experimental layout within the Astra Gemini vacuum chamber

Upon exiting the gas cell the laser was blocked with 12 μm thick sacrificial aluminium foil, and the electron beam was deflected away from the optical axis with a 15 cm long 1 T permanent dipole magnet. A scintillating Lanex screen placed in the path of the deflected electron beam recorded the electron spectrum on every shot. The x-ray beam then passed through the bone sample, which was mounted on a stage possessing 3 axis + rotation motorised degrees of freedom, and out of the vacuum chamber through a 180 μm thick beryllium window. By translating the sample along the optical axis the geometric magnification could be altered. The 20×10 mrad FWHM divergence beam of x-ray photons was deposited onto an indirect-detection camera, a scintillator fibre-coupled to a 2048×2048 pixel CCD. The x-ray spectrum was characterised by placing an 8×8 filter array of elemental metals possessing different K-edges in front of the detector. Given the known transmission through each filter it was possible to find a best-fit synchrotron spectrum for each shot, previously shown to be a good approximation to the actual spectrum[14].

Choosing Beam Parameters

This experiment considers the formation of images through absorption contrast, where the x-ray transmission of the bone (assuming a constant density throughout) varies as $e^{-\mu D}$. Here μ is the mass attenuation coefficient of the bone, and D the line-of-sight thickness of the bone at a particular pixel. The variation of D over the CCD defines a projected image of the sample, whereas the (strong) variation of μ with photon energy defines the contrast of the image. Taking both of these into account, if the photon distribution across the sample is assumed to be Poisson-like, the signal to noise ratio (SNR) can be calculated to scale like[8]

$$SNR \propto \sqrt{\frac{n\mu^2}{2De^{\mu D}}}$$

where n is the number of photons per pixel – the relative changes to SNR with sample thickness are plotted in Figure 2. For low/high photon energies the sample becomes opaque/transparent and absorption contrast signal is lost.
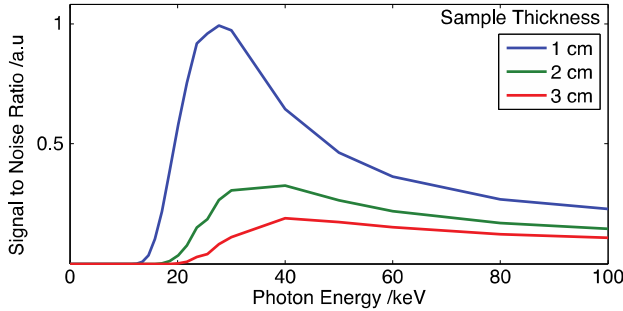
Figure 2: Relative signal-to-noise ratios in absorption contrast images as a function of bone thickness and photon energy.

Maximising this expression for a given photon flux we find an optimal $\mu \, \alpha \, D^{-1}$. As mentioned above, μ is strongly dependent on photon energy, approximately inversely proportionally, so picking an optimal μ is equivalent to using photons of an optimal energy. For our bone sample, a 7 mm diameter cylinder, the simple expression above suggests image contrast will be maximised at a photon energy of approximately 30 keV. When optimising the source in the experiment we focussed on the quality of the radiograph, achieved with a spectrum of critical energy $E_c = 36$ keV (the energy above which half of the energy is radiated in the synchrotron spectrum) – see Figure 3. Though the above estimate of photon energy is a simple one based on a monoenergetic x-ray beam, it nevertheless helps indicate the useful energy range of a broadband beam for a given sample.
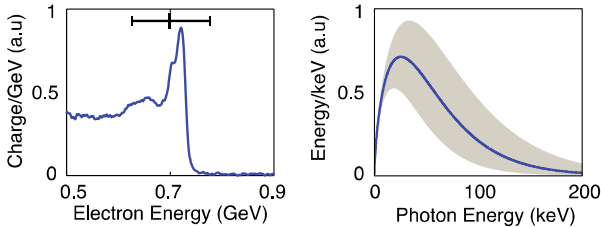
Figure 3: A measured electron spectrum and fitted photon spectrum for the radiography run, along with RMS variation in peak electron energy and photon counts.

This radiograph-centric optimisation process places less importance on perfecting the electron spectrum, reflected in Figure 3. Though it was possible to produce electron beams at energies above 1 GeV, E_c scales with the square of electron energy[15] and at this point the sample would be too transparent. The beams typically consisted of a narrow peak superimposed on a broad low energy tail. The lower energy electrons likely had little impact on the radiograph as very few would be transmitted through the sample. Over the course of the imaging runs the electron and x-ray beams remained reasonably stable, as has been observed in previous experiments using gas cells rather than gas jets[16,17] as a plasma target.

Imaging Results

After x-ray source optimisation it was possible to record many hundreds of high quality radiographs over several hours, each recorded on a single shot. One radiograph is shown in Figure 4, where the hexagonal background is a feature of the fibre-

coupling to the CCD of the camera. Individual trabeculae are clearly visible throughout, as are fine features at the edge of the sample. Limited by the physical size of the CCD and the requirement that the whole sample be visible, the effective pixel size is 4.8 μm corresponding to a geometric magnification of 2.8. Though difficult to estimate without an on-shot resolution target, examination of the edge transfer function of sharp features in the radiographs suggests a 2D resolution of approximately 40 μm. This is well above the intrinsic source size of the LWFA ($\geq$ 1 μm) and the effective pixel size, suggesting there are other factors at play affecting the final resolution.
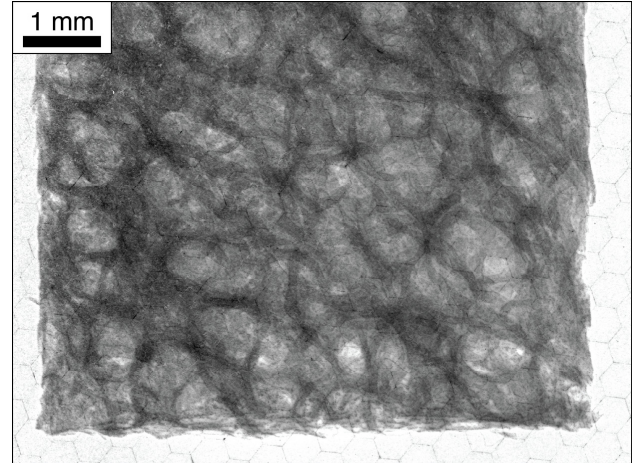
Figure 4: Example single-shot radiograph of cylindrical femoral bone sample.

One possibility is in the data analysis process – the raw CCD images suffer a number of hard photon hits, likely originating as bremsstrahlung from the dumping of the electron beam. There is necessarily a degree of spatial averaging performed when removing these hits, removing detail. As the photon flux drops at the edge of the beam the SNR drops as $n^{1/2}$, which was also observed to reduce resolution.

In a future experiment these issues could be circumvented by simply taking many shots at the same position. It is then much more likely that every pixel of the image will somewhere be unaffected by hard hits and low flux (similar to the concept of lucky imaging in astronomy).

Conclusions

We have demonstrated the capabilities of a LWFA-driven x-ray source in the context of trabecular bone imaging. Though strict demands are simultaneously placed on the source size, photon energy, photon flux, and beam stability, current results are already competitive with those obtained with microfocus x-ray sources, a field decades old. The path forward is to achieve a spatial resolution limited only by the source size, and apply the same techniques at a higher repetition rate.

Acknowledgements

References

1. Ritman, E. L. Current status of developments and applications of micro-CT. *Annu. Rev. Biomed. Eng.* **13,** 531–52 (2011).

2. Chappard, C. *et al.* Subchondral bone micro-architectural alterations in osteoarthritis: a synchrotron micro-computed tomography study. *Osteoarthr. Cartil.* **14,** 215–223 (2006).

3. Nuzzo, S., Peyrin, F., Cloetens, P., Baruchel, J. & Boivin, G. Quantification of the degree of mineralization of bone in three dimensions using synchrotron radiation microtomography. *Med. Phys.* **29,** 2672 (2002).

4. Snyder, B. & Piazza, S. Role of Trabecular Morphology in the Etiology of Age-Related Vertebral Fractures. *Calcif. Tissue Int.* **53,** 14–22 (1993).

5. Thurner, P. J. *et al.* Time-lapsed investigation of three-dimensional failure and damage accumulation in trabecular bone using synchrotron light. *Bone* **39,** 289–99 (2006).

6. Borah, B. *et al.* The effect of risedronate on bone mineralization as measured by micro-computed tomography with synchrotron radiation: correlation to histomorphometric indices of turnover. *Bone* **37,** 1–9 (2005).

7. Buckland-Wright, J. C. & Bradshaw, C. R. Clinical applications of high-definition microfocal radiography. *Br. J. Radiol.* **62,** 209–217 (1989).

8. Flynn, M. J., Hames, S. M., Reimann, D. A. & Wilderman, S. J. Microfocus X-ray sources for 3D microtomography. *Nucl. Instruments Methods Phys. Res. Sect. A Accel. Spectrometers, Detect. Assoc. Equip.* **353,** 312–315 (1994).

9. Mangles, S. P. D. *et al.* Monoenergetic beams of relativistic electrons from intense laser-plasma interactions. *Nature* **431,** 535–538 (2004).

10. Faure, J. *et al.* A laser-plasma accelerator producing monoenergetic electron beams. *Nature* **431,** 541–544 (2004).

11. Geddes, C. G. R. *et al.* High-quality electron beams from a laser wakefield accelerator using plasma-channel guiding. *Nature* **431,** 538–541 (2004).

12. Kneip, S. *et al.* Bright spatially coherent synchrotron X-rays from a table-top source. *Nat. Phys.* **6,** 980–983 (2010).

13. Hooker, C. J. *et al.* The Astra Gemini project -- A dual-beam petawatt Ti : Sapphire laser system. **133,** 673–677 (2006).

14. Fourmaux, S. *et al.* Demonstration of the synchrotron-type spectrum of laser-produced Betatron radiation. *New J. Phys.* **13,** 033017 (2011).

15. Esarey, E., Shadwick, B. A., Catravas, P. & Leemans, W. P. Synchrotron radiation from electron beams in plasma-focusing channels. *Phys. Rev. E* **65,** 056505 (2002).

16. Vargas, M. *et al.* Improvements to laser wakefield accelerated electron beam stability, divergence, and energy spread using three-dimensional printed two-stage gas cell targets. *Appl. Phys. Lett.* **104,** 174103 (2014).

17. Osterhoff, J. *et al.* Generation of Stable, Low-Divergence Electron Beams by Laser-Wakefield Acceleration in a Steady-State-Flow Gas Cell. *Phys. Rev. Lett.* **101,** 085002 (2008).